# Production of Polymeric Membranes Made of Polypropylene, Poly(ethylene-*co*-vinyl acetate), and Poly(vinyl alcohol)

**A. Maciel,[1] M. Aguilar,[2] A. Luis,[1] O. Manero[1]**

[1]*Instituto de Investigaciones en Materiales, Universidad Nacional Autónoma de México, AP 70-360, DF 04510, México*
[2]*Unidad de Materiales, Centro de Investigación Científica de Yucatán, AC Calle 43 No. 130, Col. Chuburna de Hidalgo, 97200, Mérida, Yucatán, México*

Received 18 April 2003; accepted 9 December 2003

**ABSTRACT:** In this study, we prepared and characterized membranes containing polypropylene, poly(ethylene-*co*-vinyl acetate) (EVA), and poly(vinyl alcohol) (PVA). The production process involved blend extrusion and calendering followed by solvent extraction by toluene and water of the EVA and PVA phases. Morphology studies involving scanning electron microscopy determined the pore size distribution at the surface and in the internal regions of the membrane. The resulting membrane properties were related to the processing variables (extension rate, process temperature, and solvent extraction methods) and blend composition. © 2004 Wiley Periodicals, Inc. J Appl Polym Sci 92: 3275–3286, 2004

**Key words:** membranes; poly(propylene) (PP); morphology; polymer blends

## INTRODUCTION

Polymeric membranes have been used extensively in gas separation operations, and their preparation involves different production processes.[1] Some of these processes include precipitation and phase inversion, such as those reported for the production of polyimide membranes[2] and others.[3] Asymmetric membranes with larger porosities in the inner part than in the surface are used in various separation processes. These membranes are prepared by precipitation from a solution of *N*-methyl pyrrolidone in water.[4] Alternatively, traditional processing methods, such as extrusion and calendering, for polymers can be used to prepare membranes, although they are not widely used. An example of these is the production of membranes made of polyolefins by coextrusion.[5] Furthermore, polymer blends have also been used in the production of membranes, and some of these polymers possess functional groups that promote adhesion between phases.[6]

The stretching of films to produce pores has been given attention in the production of polymeric membranes for ultrafiltration processes.[7] Biaxial extensional flow applied to laminated polypropylene (PP) with calcium carbonate fillers causes cracks in the region surrounding the particles, producing microporous laminates of PP.[8] It has been observed that a decrease in the particle size increases the porosity of the membrane. Other studies on polyacrylonitrile hollow fibers have shown the same result: as the stretching increases, the pore size increases as well.[9] Copolymers of ethylene–vinyl alcohol have been used in the production of high-selectivity permeable asymmetric membranes formed by a dense layer and a porous substrate.[10] Polymer blends used in the production of membranes for microfiltration have been prepared,[11] namely, poly(vinyl chloride)–poly(butadiene–acrylonitrile). Another study dealt with the preparation of PP–polyamide blends, with attention given to the effect of composition, mixing, and compatibilization.[12] In this study, the polyamide phase was the dispersed phase, which formed elongated laminates with augmented permeation.

In this study, we considered the PP–poly(ethylene-*co*-vinyl acetate) (EVA)–poly(vinyl alcohol) (PVA) system. The extrusion of this blend was followed by calendering, with the intention of producing an extensional flow in the region past the die. This type of deformation causes a uniform distribution of the dispersed phase in the edges of the stretched film, and such domains, after extraction by a solvent, produce pores located on the membrane surface. The membranes were prepared with polymer blends of PP (hydrophobic membrane support) and EVA as a dis-

*Correspondence to*: A. Maciel (macielal@servidor.unam.mx).

Contract grant sponsor: Consejo Nacional de Ciencia y Tecnologia (CONACYT); contract grant number: G27857-U (to A.M.).

**TABLE I**
**Membranes Produced with Various PP–EVA–PVA Compositions**

| Nomenclature | PP–EVA–PVA composition | Extension rate (mm/mm) | Extrusion temperature (°C) | Additional treatment |
|---|---|---|---|---|
| 1A | 50/20/30 | 0 | 225 | — |
| 1B0.9 | 50/20/30 | 0.9 | 215 | — |
| 1B1.8 | 50/20/30 | 1.8 | 215 | — |
| 2A | 50/30/20 | 0 | 225 | — |
| 2A0.9 | 50/30/20 | 0.9 | 225 | — |
| 2A4.1 | 50/30/20 | 4.1 | 225 | — |
| 2A7.5 | 50/30/20 | 7.5 | 225 | — |
| 2A11.8 | 50/30/20 | 11.8 | 225 | — |
| 2A14.6 | 50/30/20 | 14.6 | 225 | — |
| 2ASB | 50/30/20 | 0 | 225 | Sand blasted |
| 2A14.6SB | 50/30/20 | 0 | 225 | Sand blasted |
| 2B | 50/30/20 | 0 | 215 | — |
| 2B1.8 | 50/30/20 | 1.8 | 215 | — |
| 2B3E | 50/30/20 | 0.9, 1.2, 1.8 | 215 | — |
| 2C | 50/30/20 | 0 | 205 | — |
| 3B | 50/10/40 | 0 | 215 | — |
| 3B0.9 | 50/10/40 | 0.9 | 215 | — |
| 3B1.8 | 50/10/40 | 1.8 | 215 | — |
| 4B0.9 | 40/20/40 | 0.9 | 215 | — |
| 4B1.2 | 40/20/40 | 1.2 | 215 | — |
| 4B1.8 | 40/20/40 | 0.9 | 215 | — |
| 4B3E | 40/20/40 | 0.9, 1.2, 1.8 | 215 | — |
| 5BE3 | 40/25/45 | 0.9, 1.2, 1.8 | 215 | — |
| 6B3E | 40/30/30 | 0.9, 1.2, 1.8 | 215 | — |
| 7B0.9 | 40/35/25 | 0.9 | 215 | — |
| 7B1.2 | 40/35/25 | 1.2 | 215 | — |
| 7B1.8 | 40/35/25 | 1.8 | 215 | — |
| 7B3E | 40/35/25 | 0.9, 1.2, 1.8 | 215 | — |
| 8B | 40/40/20 | 0 | 215 | |
| 8B0.9 | 40/40/20 | 0.9 | 215 | — |
| 8B1.2 | 40/40/20 | 1.2 | 215 | — |
| 8B1.8 | 40/40/20 | 1.8 | 215 | — |
| 8B3E | 40/40/20 | 0.9, 1.2, 1.8 | 215 | — |

A = 225, B = 215, and C = 205°C for several applied strains. SB = sand blasted.

persed phase;[13–18] the latter imparts flexibility and can be solvent-extracted to produce the porous material. The blend composition was related to the morphology and permeation characteristics of the membrane.

PVA has been used in the production of membranes for biomedical applications. When mixed with PP, it forms an immiscible blend.[18,19] Its hydrophilic character allows the extraction of the domains from the polymer blend with water, and in addition, it helps in the control of pore shape. Membrane characterization implies a knowledge of the morphology, pore density, porosity, and pore size distribution. Here, the pore size and density were determined by direct observation with scanning electron microscopy (SEM) and also by the bubble pressure method. The latter method is usually applied in membrane characterization to measure the pore size, when the length scales are on the order of nanometers.[20] SEM was also used to characterize the membrane morphology and to search for interconnecting paths between both sides of the membrane.[21]

## EXPERIMENTAL

### Membrane preparation

The polymers used in the preparation of the membranes were PP, EVA, and PVA. Isotactic PP from Himont (Pro-fax 6523) (Wilmington, DE) had a melting temperature of 173°C, a density of 0.9 g/cm$^3$, and a melt flow index of 4 at 230°C. EVA from Atochem (EVATANE-28-5) (Austin, TX) had a 28% vinyl acetate composition, a melting point of 76°C, a density of 0.95 g/cm$^3$, and a melt flow index of 5 at 190°C. PVA from Dupont (ELVANOL 51-05, Houston, TX) had an 87–89% hydrolysis level, a melting point of 197°C, a density of 1.3 g/cm$^3$, and a melt flow index of 6. Blends were prepared with various PP–EVA–PVA ratios. Table I shows the composition and processing variables for the obtained samples.

A Haake 257 single-screw extruder with a length to diameter ratio ($L/D$) of 25:1 working at 20 RPM was used to produce fibers 2 mm in diameter at 210°C. Subsequently, these fibers were laminated in the same

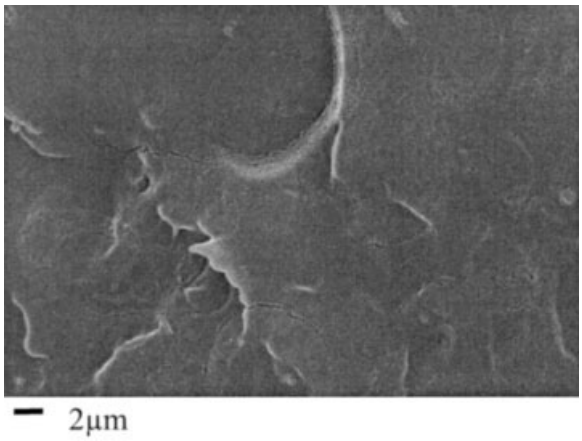


**Figure 1** Morphology of the membranes without the extraction of domains at zero strain: (a) 8B surface and (b) 2B transversal fracture (internal region).

extruder working with a temperature profile of 205, 215, and 225°C. Observation of the laminates surface revealed a skin made of PP, around 2–5 $\mu$m thick, in the upper and lower surfaces of the film. This skin impeded the appropriate distribution of pores on the surface.

To eliminate the PP at the surface, sand blast ($Al_2O_3$, with a density of 2.084 g/cm$^3$ and a particle size between 0.1 and 0.3 mm) was applied at a distance of 35 cm from the sample for 2 min with a 245 kPa pressure. PP at the surface was also removed when calendering was applied on the laminate exiting the extruder die. The mechanism by which dispersed particles migrate to regions close to the surface considers the combined shear-extensional flow produced in the die itself, enhanced by the planar extension produced by calendering at the die exit. It is expected that those particles located near the surface embedded in a predominantly PP phase may form pores on the surface after the extraction of soluble polymers.

**TABLE II**
**Influence of Extraction Time on the Amount of Extracted Polymer for the 50/20/30 PP–EVA–PVA Membranes**

| Extraction time (h) | Extracted polymer (wt %) |
|---|---|
| 4 | 24 |
| 12 | 27 |
| 24 | 30 |
| 48 | 30 |

The extractions were made with 30/70 toluene–water at 80°C.

Calendering[22] reduced the sample thickness and controlled the size of the dispersed EVA and PVA phases. At the exit of the extruder, the melted polymer velocity was on the order of 10.8 cm/min, and this increased as soon as the polymer exited the die by the action of the rollers. The roller tangential velocities considered were 30, 40, 50, 91, 154, 214, and 272 cm/min. The distance between the extruder die and the rollers was set at 21.5 cm. The strain under extensional deformation ($e$) was calculated according to the following equation:

$$e = \frac{L - L_0}{L_0} \quad (1)$$

where $L$ and $L_0$ are the final and initial separations of the reference particles in the sample. The strain values attained in the calendering process were 0.9, 1.2, 1.8, 4.1, 7.5, 11.8, and 14.6. The membrane preparation stage involved various PP–EVA–PVA compositions with several deformation rates at different temperatures.

The obtained membranes contained a matrix of PP and a dispersed phase made of EVA and PVA. The latter polymers were soluble in polar solvents; that is,

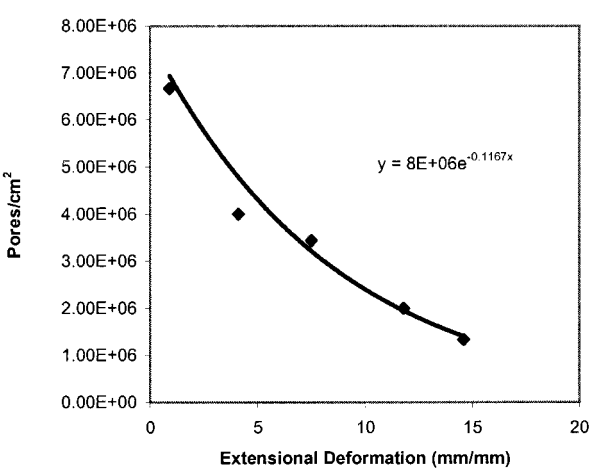


**Figure 2** $\rho$ against extensional deformation for the 50/30/20 PP–EVA–PVA composition at 225°C. The density of pores decreased as a single exponential function.

**TABLE III**
**Extracted Polymer Amounts for 50/30/20 PP–EVA–PVA Membranes at Various Strains**

| Membrane | Tangential velocity (cm/min) | Thickness (mm) | Extracted polymers (%) |
|---|---|---|---|
| 2A0.9 | 30 | 0.56 | 22 |
| 2A4.1 | 91 | 0.37 | 24 |
| 2A7.5 | 154 | 0.31 | 32 |
| 2A11.8 | 214 | 0.23 | 33 |
| 2A14.6 | 272 | 0.14 | 33 |

| Membrane | Tangential velocity (cm/min) | Thickness (mm) | Extracted polymers (%) | | | | |
|---|---|---|---|---|---|---|---|
| | | | 4 h with water | 48 h with toluene | 4 h with water | 48 h with toluene | Total |
| 2A0.9 | 30 | 0.56 | 3 | 7 | 7 | 13 | 30 |
| 2A4.1 | 91 | 0.37 | 4.5 | 10.5 | 0.5 | 18.5 | 34 |
| 2A7.5 | 154 | 0.31 | 5 | 14.5 | 3 | 14.5 | 37 |
| 2A11.8 | 214 | 0.23 | 3.5 | 10 | 3.5 | 16 | 38 |
| 2A14.6 | 272 | 0.14 | 3 | 16 | 3.5 | 16.5 | 38.5 |

The upper part of the table shows polymers extracted with a toluene–water emulsion at 80°C for 24 h. The lower part of the table shows polymers that underwent two successive extractions, first, with water at 90°C for 4 h and, then, with toluene at room temperature for 48 h.

PVA was soluble in water, and EVA was soluble in toluene. Two different methods of extraction were tested, namely, emulsion extraction and single-solvent extraction. In the first method, water–toluene emulsions were used at various temperatures for several extraction times. In the second method, successive extractions with water and toluene separately were implemented. Membranes were submerged in water at 90°C for 4 h, and subsequently, they were submerged in toluene at room temperature for 24 h. The same procedure was repeated again for a total of four extractions. The polymer weight extracted was measured at every stage to correlate these data with the extensional deformation in the calendering process and with the extrusion temperature of the material. The water and toluene solutions formed by the extractions stages were analyzed with IR spectroscopy.

Determinations of the pore radius ($r$) were carried out with the bubble point method according to the Cantor equation:

$$r = \frac{2\gamma}{\Delta p} \tag{2}$$

where $\gamma$ is the surface tension and $\Delta p$ is the pressure gradient. In this method, the membrane is located in

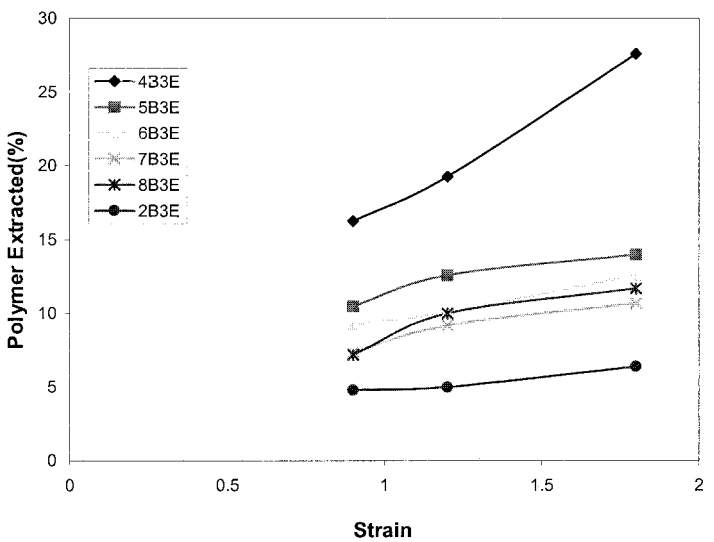


**Figure 3** Polymers extracted with water in the first step as a function of the roller tangential velocity for various membranes. A high PVA content allowed a larger extraction with water.

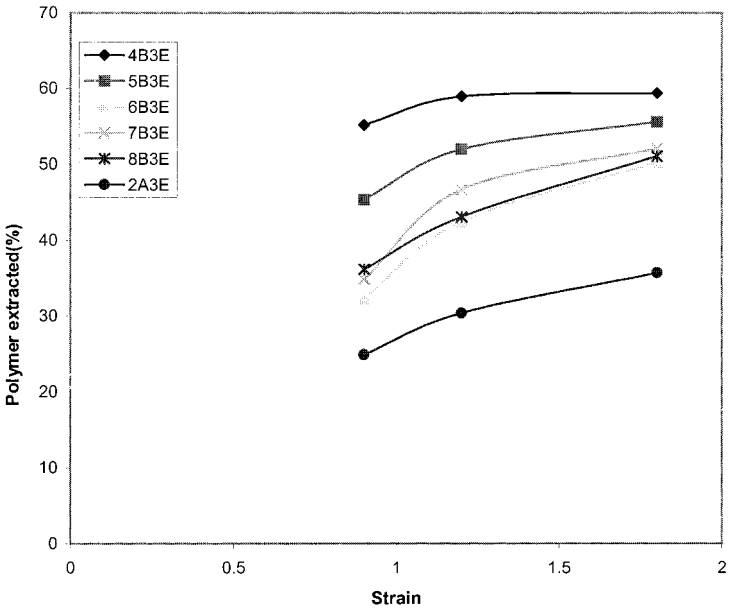


**Figure 4** Total polymer extraction for several membranes after four extraction stages. The lowest amount of extracted polymers corresponded to the membrane with the smallest amount of soluble polymers.

the middle of a vertical cylindrical reservoir. The upper part of the container is filled with water in contact with the membrane. A stream of air is fed from the lower part of the container. The pressure needed to produce the first bubble on the upper part of the membrane is measured. The density of pores (pores/area) was determined by direct observation by SEM over an area of 1948 $\mu m^2$. An image analyzer (Image ProPlus 3.0, Silver Spring, MD) was used to build the size frequency histograms. Special attention was given to the distribution of the largest pores in the membranes, included in the insets of some of the plots. Because the largest pores represented a small proportion of the total number of pores, a restriction was imposed to large particles. After the polymer solvent-extraction stage, the external surface of the membranes was observed to determine the density of pores on the surface ($\rho$), and also, the samples were cut transversely with cryogenic fracture to observe the inner porosity of the membranes. The samples were gold-covered before optical microscopy observations (Leica Stereoscan 440, Cambridge, UK). Once the pore density was determined, the surface porosity ($\epsilon$) was calculated according to the following equation[23]

$$\epsilon = \rho \pi d_p^2/4 \tag{3}$$

where $d_p$ is the average diameter of the pores. The empty space (ES) was determined from the density and weight measurements of the extracted polymers with the equation

$$\mathrm{ES} = \frac{V_{\mathrm{EVA}} + V_{\mathrm{PVA}}}{V_{\mathrm{PP}} + V_{\mathrm{EVA}} + V_{\mathrm{PVA}}} \tag{4}$$

Here, the volume of the soluble polymers poly(ethylene-*co*-vinyl acetate) and poly(vinyl alcohol) ($V_{\mathrm{EVA}}$ and $V_{\mathrm{PVA}}$, respectively) was divided by the total volume of polymers in the membrane, including the volume of polypropylene ($V_{\mathrm{PP}}$).

The total porosity (TP) is the sum of $\epsilon$ and ES:

$$\mathrm{TP} = \epsilon + \mathrm{ES} \tag{5}$$

The standard deviation ($\sigma$) of the pore diameter was calculated as follows:

$$\sigma = \sqrt{\frac{\sum (y - n)^2}{N}} \tag{6}$$

where $y$ is the diameter of the pores, $n$ is the diameter mean, and $N$ is the total number of pores in the analyzed area.

## RESULTS AND DISCUSSION

### Morphology of the membranes without domain extraction

The surface morphology of the membranes without domain extraction is shown in Figure 1(a), which reveals absence of porosity on the surface. The internal morphology (transversal surface) is shown in Figure 1(b), which shows the presence of particles and holes. After cryogenic fracture, the opposing surfaces were exposed and voids and particles appeared.

### Extraction studies

Considering that the theoretical amount of extractable polymers is the percentage in weight of EVA and

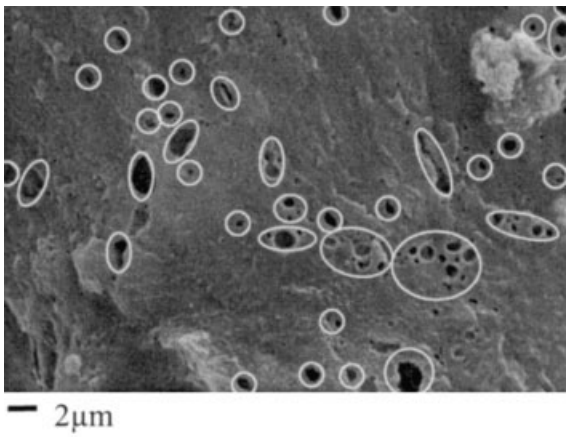


**Figure 5** Morphology of the membranes after domain extraction at zero strain: (a) 8B surface and (b) 2B transversal fracture (internal region).

PVA, we evaluated the efficiency of the extraction methods. Initially, it was necessary to determine the influence of extraction time on the resulting EVA and

**TABLE IV**
**Pore Statistics for Membranes Produced at Zero Strain After Domain Extraction from the Surface (8B) and from the Internal Part (2B)**

| Membrane | 8B surface | 2B inner region |
|---|---|---|
| $d_p$ ($\mu$m) | 0.28 | 3.17 |
| $\sigma$ ($\mu$m) | 0.17 | 3.03 |
| Minimum ($\mu$m) | 0.03 | 0.02 |
| Maximum ($\mu$m) | 4.1 | 5.3 |
| $N$ | 91 | 581 |

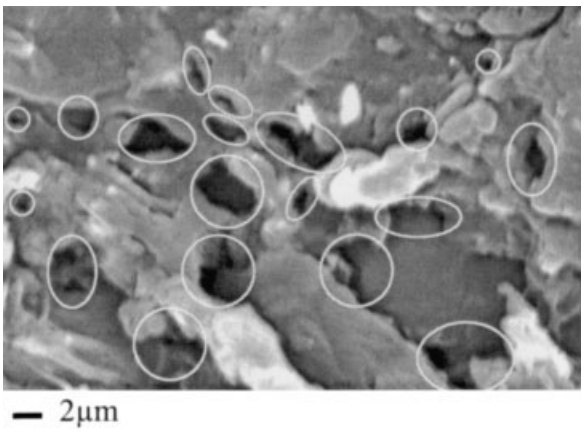


**Figure 6** Morphology of the 50/30/20 PP–EVA–PVA membrane subjected to sandblasting. The pore size increased with abrasion.

PVA weight extracted from the membrane, especially in the first extraction method with emulsion. As shown in Table II, up to 30% of the initial weight was extracted from membrane 1A (see Table I for sample identification) without stretching. In this case, an emulsion of 30/70 toluene–water was used at 80°C. Although it was possible to extract the whole amount of PVA and EVA, the morphology of the sample restricted the extraction, thus causing some of the microdomains to remain trapped in the PP matrix.

Figure 2 shows the pore density as a function of extensional deformation for a membrane with 50/30/20 PP–EVA–PVA composition at 225°C. Interestingly, the pore density decreased as a single exponential function with strain, in agreement with the flow behavior of the dispersed domains under extensional flow. Additional data taken at a lower temperature (215°C) at a constant strain of 0.9 showed a higher pore density ($\sim 1 \times 10^7$ pores/cm$^2$). A higher strains allowed a larger proportion of extracted polymers. In

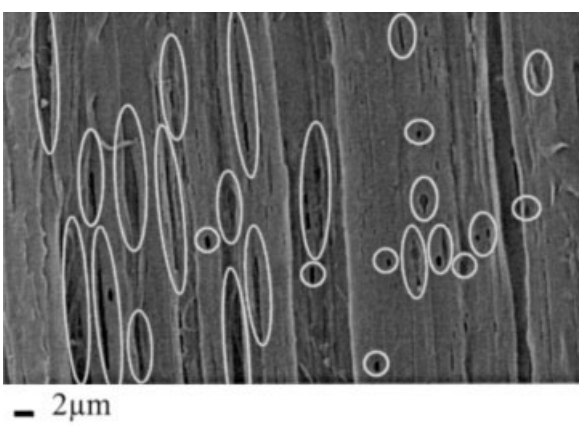


**Figure 7** Maximum domain deformation for the 50/30/20 PP–EVA–PVA membrane (strain = 14.6).

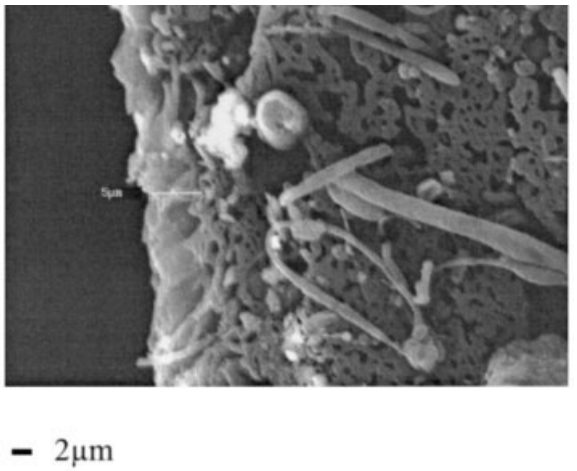


**Figure 8** Transversal view of the 50/30/20 PP–EVA–PVA membrane (a) after immersion in toluene and (b) after immersion in toluene and water. EVA and PVA were extracted selectively.

the upper part of Table III, the data are displaced for the extracted polymers from a 50/30/20 PP–EVA–PVA membrane by a 70/30 toluene–water emulsion at 80°C for various strain values. The total polymer extraction was low for small strains but increased as strain augmented, becoming constant for higher deformations. In the lower part of Table III, the results are shown for the second extraction method (with successive extractions), first with water at 90°C for 4 h, and then with toluene at ambient temperature for 48 h. These two stages were repeated for four successive steps. The results reveal that the extraction process was dependent on the interfacial tension. For water at 90°C, the interfacial tension was 60.75 dyne/cm, and for toluene at 20°C, the interfacial tension was 28.4 dyne/cm.[24] The extraction of EVA with toluene was more efficient because of similar solubility parameters (18.6 $MPa^{1/2}$ for EVA and 18.2 $Mpa^{1/2}$ for toluene)[25]

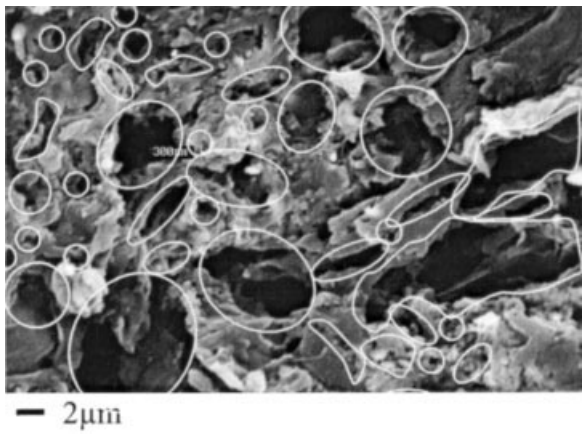


**Figure 9** 50/30/20 PP–EVA–PVA membrane treated with sandblasting. It showed larger pores and a higher size dispersion because of abrasion.

than the extraction of PVA with water (25.9 $MPa^{1/2}$ for PVA and 47.9 $MPa^{1/2}$ for water). The IR analysis confirmed that the extractions were attained selectively. Water was used to extract PVA, and toluene was used to extract EVA.

Figure 3 shows the percentage of polymers extracted with water during the first extraction stage as a function of strain for various membranes extruded at 225°C. This first extraction stage was related to the PVA content on the membranes surface and, thus, was also related to the porosity generation in the PP layer. The blend with 40/20/40 PP–EVA–PVA (the highest PVA proportion) presented the highest extraction in water, which increased with strain. In the other systems, the extraction amount augmented slowly with strain. In Figure 4, the total polymer extraction after four extraction stages is presented as a function of strain. Once again, higher extractions were obtained with larger strain. The sample with 40% PVA showed the highest amount of extracted EVA and PVA. However, the sample with 50/30/20 PP–EVA–PVA pre-

**TABLE V**
**Pore Diameter and $\rho$ for Membranes Produced at Strains of 0.9, 1.2, and 1.8 for various Compositions**

| Membrane | Average pore diameter (direct observation; $\mu$m) | $\rho$ (pores/$cm^2$) |
|---|---|---|
| 4B0.9 | 0.65 | $5.40 \times 10^6$ |
| 4B1.2 | 0.54 | $1.95 \times 10^7$ |
| 4B1.8 | 0.43 | $1.36 \times 10^7$ |
| 7B0.9 | 0.78 | $1.21 \times 10^7$ |
| 7B1.2 | 0.7 | $6.90 \times 10^6$ |
| 7B1.8 | 0.65 | $6.10 \times 10^6$ |
| 8B0.9 | 0.6 | $5.24 \times 10^6$ |
| 8B1.2 | 0.85 | $1.16 \times 10^7$ |
| 8B1.8 | 0.7 | $7.44 \times 10^6$ |

$\rho$ values were determined from direct observation of the micrographs.

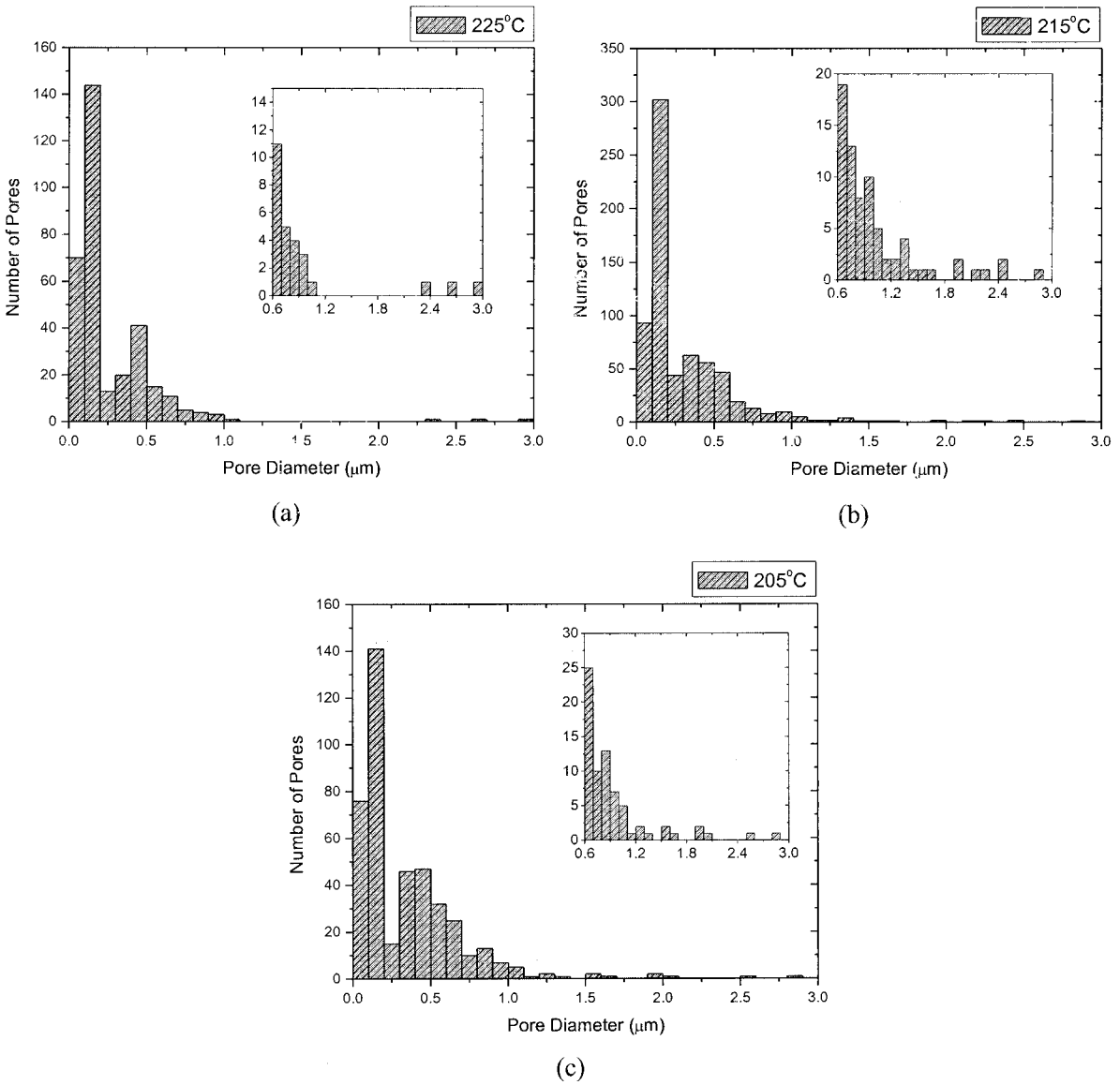


**Figure 10** Distribution of pores on the surface of the 50/30/20 PP–EVA–PVA membrane (strain = 0.9 mm/mm) at (a) 225, (b) 215, and (c) 205°C. The larger porosity was obtained at 215°C.

sented the lowest proportion of extracted polymers because of a lower soluble polymer content.

## Morphology studies of the extracted blends

The resulted surface morphology of membrane 8B after polymer extraction obtained at zero strain is shown in Figure 5(a). The membrane presented a non-uniform distribution of pore sizes. However, the inner part of the membrane [labeled 2B and shown in Fig. 5(b)] presented a more regular distribution of pore sizes (between 0.02 and 5.9 $\mu$m). Table IV shows the pore statistic for both cases.

The morphological features of the 2ASB membranes prepared by the extraction of soluble polymers with toluene–water at zero strain are shown in Figure 6. The pores sizes ranged from 0.5 to 9 $\mu$m. Sandblasting eroded the skin of the membrane and allowed us to observe the internal porosity. The pore size was suitable for ultrafiltration uses if the membrane presented interconnection between the two sides. When extensional flow was applied, the morphology of the membranes depended on strain. At low strains, the dispersed phase was composed of circular domains. As the strain increased, most of the domains acquired an elongated shape in the flow direction. The maximum deformation of the domains was attained in membrane 2A14.6, as shown in Figure 7. The size of these domains was between 0.3 and 10 $\mu$m, as illustrated in the micrograph with white circles. The big channels were defects of the membrane generated by microdo-

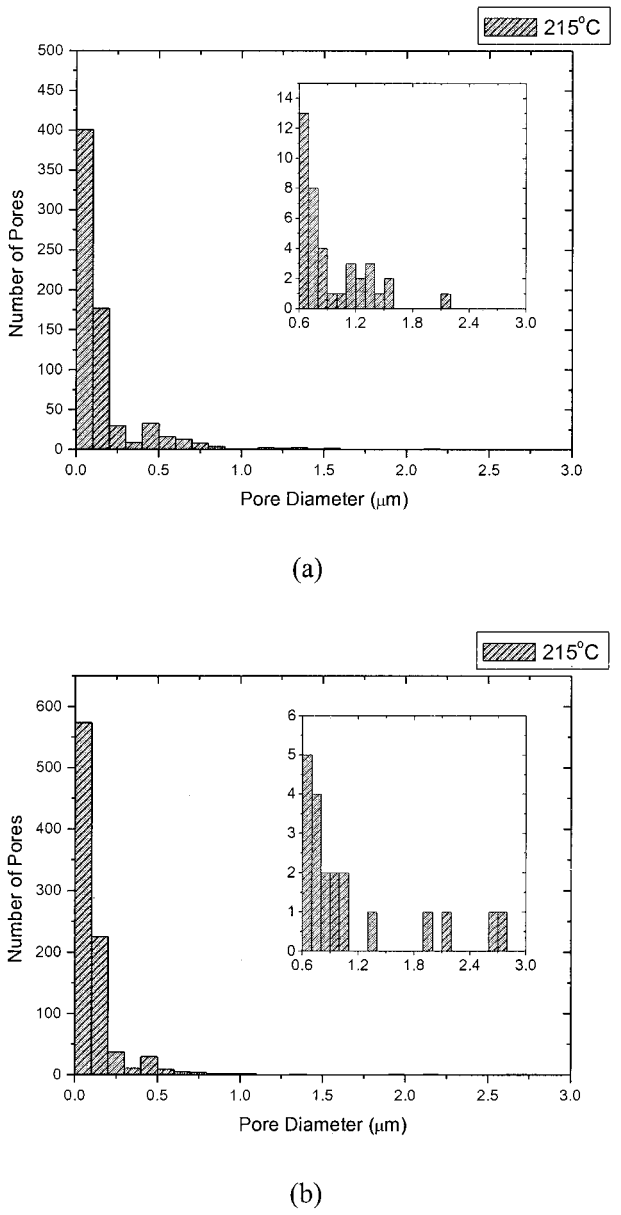


**Figure 11** Surface pore distribution for various membranes at 215°C (strain = 0.9) for membranes with the following PP–EVA–PVA compositions: (a) 50/20/30 and (b) 50/10/40. When PVA was added, the pore density increased.

mains of the dispersed phase on the surface during the calendering process.

The extrusion temperature influenced the morphology of the membrane but not the pore size. Membranes obtained at 215°C presented a larger number of pores on the surface per unit area, independently of the blend composition. In these membranes, the size of the pores on the surface and the size of the inner pores were not the same. Such features are characteristic of asymmetric membranes. In fact, the size of the inner pores was 1–9 $\mu$m. The pores on the surface were smaller because they were produced by PVA microdomains that moved to the surface during the calendering process.

**TABLE VI**
**Surface Pore Statistical Analysis for the 50/30/20 PP–EVA–PVA Blends Produced at Different Temperatures**

| | Temperature (°C) | | |
|---|---|---|---|
| | 205 | 215 | 225 |
| $d_p$ ($\mu$m) | 0.35 | 0.31 | 0.27 |
| $\sigma$ ($\mu$m) | 0.37 | 0.37 | 0.30 |
| Minimum ($\mu$m) | 0.05 | 0.05 | 0.05 |
| Maximum ($\mu$m) | 2.9 | 5.37 | 2.94 |
| $N$ | 430 | 687 | 332 |

Figure 8 shows the transversal view of blend 2A14.6 after immersion in toluene alone [Fig. 8(a)] and in toluene and water [Fig. 8(b)]. In these photographs, an external layer 2–5 $\mu$m wide and an internal region of the membrane can be seen clearly, which depicts the interconnected porous domains. As shown in Figure 8(a), fibrous structures made of PVA still prevailed after toluene immersion, but they disappeared after immersion in water at 90°C, as shown in Figure 8(b). Importantly, extensional flow allowed the formation of microdomains at the surface in one process stage, thinning the membrane and promoting permeability. When these membranes were treated by sandblasting, the size of pores on the surface increased in number, and pore size polydispersity augmented (0.3–10 $\mu$m), as shown in Figure 9.

As shown in Figure 8(a,b), the membranes were formed by a dense surface region in contact with a highly porous internal core, which allowed high selectivity and variable permeability. In this asymmetric pattern, the largest resistance to diffusion of species was concentrated in the outer region of the membrane.[6]

## Pore statistics

Table V presents a list of blends processed at several strains, and for each blend, the resulting pore size and pore densities per unit area are shown. The pore size,

**TABLE VII**
**Surface Pore Statistical Analysis for Membranes Produced with 50% PP and Several EVA and PVA Concentrations and Extruded at 215°C**

| | PVA (wt %) | | |
|---|---|---|---|
| | 20 | 30 | 40 |
| $d_p$ ($\mu$m) | 0.31 | 0.18 | 0.12 |
| $\sigma$ ($\mu$m) | 0.37 | 0.47 | 0.21 |
| Minimum ($\mu$m) | 0.03 | 0.03 | 0.03 |
| Maximum ($\mu$m) | 5.37 | 7.2 | 2.73 |
| $N$ | 687 | 710 | 913 |

Strain = 0.9.

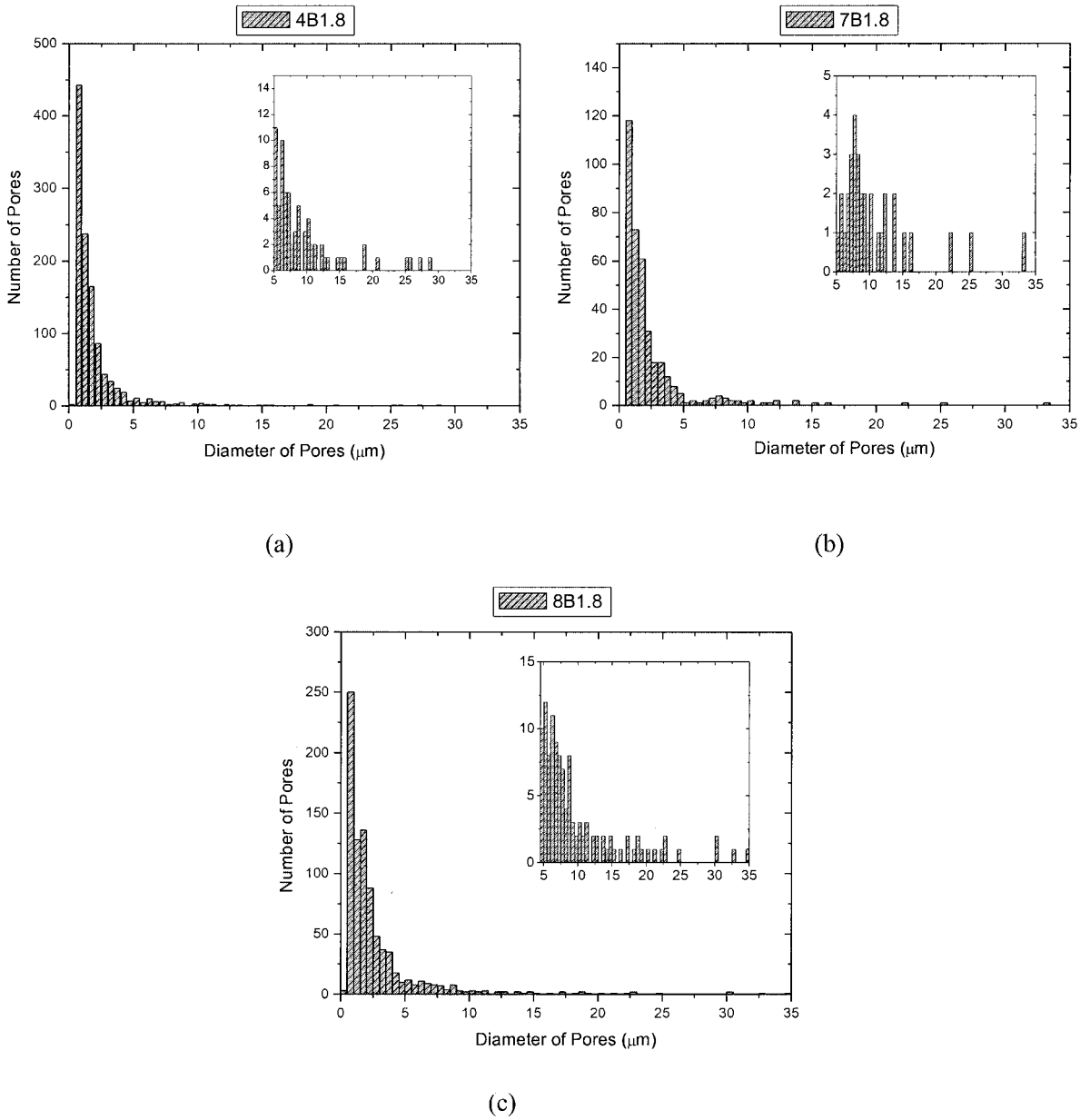


**Figure 12** Internal pore distribution for several membranes at 215°C (strain = 1.8): (a) 4B1.8, (b) 7B1.8, and (c) 8B1.8. When the PVA content was increased, the number of pores in the internal region diminished.

as determined from direct observation of the micrographs, was in the range 0.4–0.8 $\mu$m. A high pore density was obtained when the PVA content in the blend was large. Interestingly, the determinations of the pore diameter by the bubble point method gave much higher values, on the order of 5–30 $\mu$m. The two methods differed largely in their results, and one reason disagreement occurred is that the high pressure used in the bubble point method may have deformed and increased the size of the pores. In Figure 10(a–c), the surface pore distribution is shown for the 50/30/20 PP–EVA–PVA blend processed at three temperatures. In these three cases. the most frequent pore diameter was 0.2 $\mu$m, but the total number of pores was higher when the blend was processed at 215°C. At this temperature, the PVA particles migrated to the surface of the sample more efficiently. In addition, there was a slight trend toward smaller sizes with increasing temperature, which reflected a smaller number of dispersed particles as the temperature was increased.

As shown in the insets of Figure 10, the larger pore diameter gave information on the maximum particle size that the membrane could separate. The insets in Figures 10 and 11 magnify the pore distribution between 0.5 and 3.0 $\mu$m. Three samples were analyzed for each membrane. Table VI shows the statistical analysis of the data shown in Figure 10(a–c). At 215°C,

the largest pore number was obtained. This temperature was close to the melting temperature of PP (173°C) and to that of PVA (197°C). Under these conditions, the PVA domains were hard enough to penetrate the soft and low-viscous PP film, which formed the skin of the membrane.

In Figures 10(b) and 11(a,b), we compare the effect of various PVA contents on the surface pore distribution for membranes 1B0.9, 2B0.9, and 3B0.9, with the PP concentration constant (50%). Table VII summarizes the statistical data. The pore number increased with PVA content, but the mean diameter diminished considerably. This behavior could be ascribed to the decreasing EVA content, which led to an increasing viscosity of the blend. Higher viscosity implies larger shear stresses that produce more accentuated particle breakup and, hence, smaller domains.[26]

Finally, in Figure 12(a–c) and in Table VIII, we show the pore size distribution of the inner part of membranes 4B1.8, 7B1.8, and 8B1.8 containing various proportions of EVA and PVA, with the PP content constant (40%). The experimental error in the pore diameter was 3% for the latter figures. The inset magnifies the pore size distribution between 5 and 35 $\mu$m. In contrast to previous data, in this case the pore size was centered between 0.5 and 1 $\mu$m, and the frequency diminished considerably for pore sizes larger than 5 $\mu$m. The mean pore diameter diminished as the PVA content rose, which was consistent with the high viscosity in the blend, which induced a larger deformation and break up of the domains. This explains why the pore diameters on the membrane surface reported in Table IV were smaller than those pores sizes reported in Table VIII for the internal part of the membrane. Higher stresses developed at the membrane surface in the combined extrusion calendering process.

### Porosity

The membrane porosity per unit area was measured at the surface of the sample, but the TP was determined with the weight of extracted polymers considered. The results of these determinations are given in Table IX. As shown, the lowest $\epsilon$ belonged to the blend with 40% PVA. In contrast, this membrane had the largest internal porosity and the largest TP.

**TABLE VIII**
**Internal Pore Statistical Analysis for Membranes Produced with 40% PP at 215°C**

| | Membrane | | |
|---|---|---|---|
| | 4B1.8 | 7B1.8 | 8B1.8 |
| $d_p$ ($\mu$m) | 2.12 | 2.59 | 2.78 |
| $\sigma$ ($\mu$m) | 3.58 | 3.88 | 3.75 |
| Minimum ($\mu$m) | 0.02 | 0.02 | 0.02 |
| Maximum ($\mu$m) | 2.8 | 3.3 | 3.5 |
| $N$ | 114.1 | 379 | 860 |

Strain = 1.8.

**TABLE IX**
**Surface and Total Porosity for Several Membranes at Low Extensional Deformations**

| Membrane | Pores on the surface $\epsilon$ ($cm^2/cm^2$) | Total porosity ($cm^3/cm^3$) |
|---|---|---|
| 4B0.9 | $1.80 \times 10^2$ | 0.5520 |
| 4B01.2 | $4.46 \times 10^2$ | 0.5898 |
| 4B1.8 | $1.97 \times 10^2$ | 0.5945 |
| 7B0.9 | $5.78 \times 10^2$ | 0.2882 |
| 7B1.2 | $2.66 \times 10^2$ | 0.4129 |
| 7B1.8 | $2.02 \times 10^2$ | 0.4621 |
| 8B0.9 | $1.48 \times 10^2$ | 0.3152 |
| 8B1.2 | $6.58 \times 10^2$ | 0.4053 |
| 8B1.8 | $2.86 \times 10^2$ | 0.4719 |

The total surface porosity of the membrane with 40% PVA was the lowest. In contrast, this membrane had the largest internal and total porosity.

## CONCLUSIONS

The processes analyzed in this study allowed us to prepare symmetric and asymmetric porous membranes. The EVA proportion in the blends promoted a more regular pattern in the internal morphology of the membranes. With high PP contents (more than 50%), the extraction of soluble polymers was more efficient for the EVA phase because of the lower interfacial tension of toluene and the similarity of the solubility parameters of EVA and toluene. We have shown that the process of successive extractions of EVA and PVA with toluene and water separately was more efficient than that with a toluene–water emulsion.

$\epsilon$ per unit area increased more than 30% as the PVA content of the blend increased from 20 to 40%. Porosity values of more than 70% were obtained at 215°C, and the extensional flow produced by calendering diminished $\epsilon$ as a single exponential function. The resulting pore size was increased largely with the sandblasting process.

The authors thank Jose Guzman, Ernesto Sanchez, Wilberth Herrera Kao, Ma Teresa Vazquez, Sara Jimenez, Fernando Silvar, and Ivan Puente for their technical support. The authors also thank Veronica Salas and Hector Berger.

### References

1. Kesting, R. E.; Fritzsche, A. K. Gas Separation Membranes; Wiley: New York, 1993.
2. Pérez, S.; Merlen, E.; Robert, E.; Cohen Addad, J. P.; Viallat, A. J Appl Polym Sci 1993, 47, 1621.
3. Byun, S. H.; Burford, R. P. J Appl Polym Sci 1994, 52, 813.

4. Staude, E.; Breitbach, L. J Appl Polym Sci 1991, 43, 559.
5. Compañ, V.; Andrio, A.; López, M. L. Polymer 1996, 37, 5831.
6. Salamone, J. C. Polymeric Materials Encyclopedia; CRC: New York, 1996; Vol. 7.
7. Nago, S.; Nakamura, S.; Mizutani, Y. J Appl Polym Sci 1992, 45, 1527.
8. Nago, S. Mizutani, Y. J Appl Polym Sci 1998, 68, 1543.
9. Yang, M. C.; Chou, M.-T. J Membr Sci 1992, 25, 163.
10. Nakamae, K.; Miyata, T.; Matsumoto, T. J Membr Sci 1992, 25, 163.
11. Islam, M. A.; Stoicheva, R. N.; Dimov, A. J Membr Sci 1996, 118, 9.
12. Holsti-Miettinen, R. M.; Perttilä, K. P.; Seppälä, J. V.; Heino, M. T. J Appl Polym Sci 1995, 58, 1551.
13. Thomas, S.; Gupta, B. R.; De, S. K. Polym Degrad Stab 1987, 18, 189.
14. Thomas, S. Mater Lett 1987, 5, 360.
15. Ramírez-Vargas, E.; Navarro-Rodríguez, D.; Medellín-Rodríguez, F. J.; Heurta-Martínez, B. M.; Lin, J. S. Polym Eng Sci 2000, 40, 2241.
16. Gupta, A. K.; Ratnam, B. K.; Srinivasan, K. R. J Appl Polym Sci 1992, 45, 1303.
17. Thomas, S.; George, A. Eur Polym J 1992, 28, 1451.
18. Maciel, A.; Del Real, A.; García-Garduño, M. V.; Olivia, E.; Manero, O.; Castaño, V. M. Polym Int 1996, 41, 227.
19. Lohfink, G. W.; Kamal, M. R. Polym Eng Sci 1993, 33, 1404.
20. Yeo, J. H.; Lee, C. H.; Park, C.-S.; Lee, K.-J.; Nam, J.-N.; Kim, S. W. Adv Polym Technol 2001, 20, 191.
21. Law, S. J.; Mukhopadhyay, S. K. J Appl Polym Sci 1996, 62, 33.
22. Kamal, M. R.; Tan, V. Polym Eng Sci 1979, 19, 558.
23. Tanner, R. I. Engineering Rheology; Clarendon: New York, 1998.
24. Synthetic Polymer Materials; Kesting, R. E., Ed.; McGraw-Hill: New York, 1971.
25. Perry, J. H. Manual del Ingeniero Químico; Unión Tipográfica Editorial Hispano-Americano: México City, 1980.
26. Brandrup, J.; Immergut, E. H.; Grulke, E. A. Polymer Handbook; Wiley: New York, 1999; Chapter 7.
27. Maciel, A.; Salas, V.; Guzman, J.; Manero, O. J Polym Sci Part B: Polym Phys 2002, 40, 303.